AARHUS UNIVERSITY

Enhancing solar cell efficiency: an optimization of up-converting materials

Author:
Harish Lakhotiya

Supervisors:
Brian Julsgaard
Peter Balling

in the

Semiconductor Group
Department of Physics and Astronomy

September 2016

_____-

Abstract

In crystalline Si solar cells, an absorption of 1500 nm wavelength light is not possible because its corresponding energy is below the band gap of the Si.Therefore its upvconversion into 980 nm wavelength makes it available energy. However, a small absorption cross section of Er^{3+} limits the efficiency of the upconversion process.The plasmonic enhancement of upconversion process, by placing Au nanostructures nearby Er^{3+} ions, at 1500 nm wavelength is important but not much work has been reported. Therefore, there is a strong need to explore the plasmonic enhancement of upconversion at the 1500 nm wavelength.

My PhD research deals with the optimization of the upconversion process for the 1500 nm excitation wavelength by the selection of a host material for the Er^{3+} ions, and the optimization of the plasmonic nanostructures. I demonstrate upconversion of 1500 nm wavelength light using Er^{3+} emitters doped in a TiO_2 matrix and enhancement of the upconversion luminescence using Au nanodiscs. The geometric parameters of the Au nanodiscs have been engineered to achieve a maximum extinction at the excitation wavelength based on design inputs from a simulation study using a finite element modelling (FEM) approach. The experimental work has shown a reasonable agreement with the FEM except the points where the experimental results show the presence of the inter-plasmon (Au-Au)interactions. The experimentally achieved enhancement in upconversion luminescence is in good agreement with the FEM results, but differs by a factor of 3 quantitatively, indicating a need for further refinement in the simulation model. Exploring nanostructures as an another host, the study of the plasmonic assisted upconversion process in commercial $NaYF_4$ nanocrystals (mean size $\sim$ 20 nm) doped with Er3+ emitters has been performed. A rigorous process of optimization of the coating method was carried out to obtain crack-free thin films of $NaYF_4$ nanocrystals. A random array of Au nanodiscs has been deposited on top of the UCNP film for further enhancement in the upconversion process. In addition, I have also chemically linked the commercial Au nano-rods, which give a plasmon resonance peak at 1500 nm wavelength, with the $NaYF_4$ nanocrystals to fabricate a plasmon embedded upconverting thin film. A high degree of upconversion enhancement can be achieved due to the nearly equivalent local field distribution around all the Er^{3+} emitters.

In the near future, my focus will be on the chemical synthesis of highly efficient upconverting nanoparticles (UCNP) and tailoring their emission properties. In the final year of my PhD, I aim to assemble a highly optimized plasmonically enhanced upconverting layer with the currently available bifacial silicon and organic solar cells to study the influence of upconversion on the photovoltaic conversion efficiency.

Contents

Chapter 1

Introduction

It has been reported that sun light, which arrives on the surface of the earth, delivers 10,000 times the world energy demand[1, 2]. As a result, the use of solar energy has the potential to meet a large portion of future energy requirements. Si is an attractive materials for the solar industry due to the high abundance and non-toxic nature. Today, around 93 percent of total PV industries are based on Si-technology. Despite a significant development of the solar cell industry, efficient and cost-effective solar energy conversion is still a daunting task[3–5]. One of the main reasons for the poor efficiency is a spectral mismatch between the very wide spectrum of photon energies in the sun light and the band-gap energy of the solar cell material[6]. When photons with energy lower than the band gap of the absorbing materials strike the surface of a solar cell, it simply passes through without being able to generate electron-hole pair in the material. These losses of photons are called sub-band gap or transmission losses. On the other side, photons with energy higher than band gaps are even able to generate electron-hole pair but loose the excess energy in form of heat and such losses are called thermalization losses. The contribution of these sub-band gap losses in a single junction crystalline-Si solar cells are around 20 percent whereas thermalization losses cover almost 30 percent of the total losses[7]. This binds the theoretical efficiency of a crystalline-Si solar cell at 32 percent, also called Shockley-Queisser limit. However control of these losses could further increase the S-Q limits for such devices.

1.1   Motivation

One of the ways to reduce the sub-band gap or transmission losses of solar cells is to upgrade the low energy photons into high energy photons as depicted in figure 1.1(a). This process of conversion of two low energy photons into one high energy photon is called upconversion. Upconversion is also known as anti-stokes emissions as it violates the stoke emission law where emission energy must be lower than the absorption energy. It is shown that some lanthanide with partially filled 4f shell embedded in solids, may easily deviate from the stokes law and produce emission energy higher than excited energy on a moderate to a strong laser pump power [8]. In crystalline Si solar cells, an absorption of 1500 nm wavelength light is not possible because its corresponding energy is below the band gap of the Si.Therefore its upvconversion into 980 nm wavelength makes it available energy. However, a small absorption cross section and partly forbidden transition among 4f energy states in lanthanide limit the efficiency of the upconversion process.
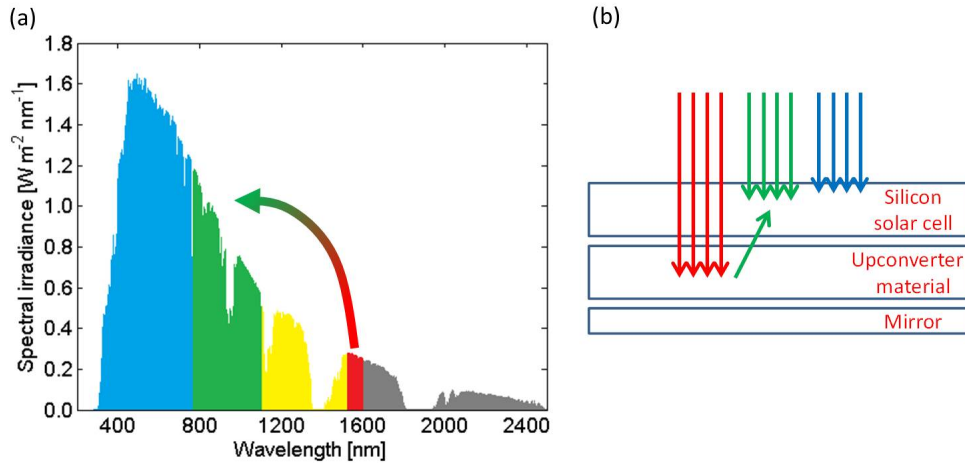
Figure 1.1: Solar spectrum and upconverted solar cell (a) The conversion of 1500 nm wavelength into 800-1000 nm spectral range in AM 1.5 solar spectrum. This process is called upconversion (b) It shows a sketch of a silicon solar cell assembly with upconverting layer at the back.

It has been shown that the upconversion enhancement can be effectively achieved by placing metal nanostructures close to Er^{3+} emitters[9–12]. However, seeing the importance of the plasmon enhanced upconversion of 1500 nm wavelength in C-Si solar cell, a complete study is ill-reported. Therefore, there is a strong need to explore the plasmonic enhancement of upconversion at the 1500 nm wavelength. J. Goldschmidt et al. [13, 14] have reported a simulation study using a simple spherical geometry of a plasmon. However, local field is more enhanced in the presence of sharp edges in a plasmonic nanostructure compared to a complete lack of edges[15]. Therefore, a study of the complex geometries of plasmonic nanostructures is required to gather realistic information on the potential for enhancement of efficiency at the 1500 nm wavelength as well as for controlling the configuration of nanostructures to achieve the said efficiency.A careful design of metallic structure is a pre-requisite for an efficient enhancement at a desired wavelength [16, 17]. Implementation of such plasmon enhanced upconverting thin films behind commercially available solar cells as shown in figure 1.1(b) could make them more efficient than the present case.

1.1.1   Upconversion and process mechanisms

Upconversion process requires at least two photons to be absorbed of near infra red to get emitted one visible photon.This process is strongly depend upon the intensity of the incoming light. The emitted light has following dependence on the incoming light [10,18]

$$I_{UC} \propto I_{in}^n, \tag{1.1}$$

In the weak pumping power regime, n shows the number of the photons require to populate the excited states [18]. Therefore n = 2 for the two photon upconversion process. The excited states get saturates with electrons once pumping power raises to high limits and that in results,
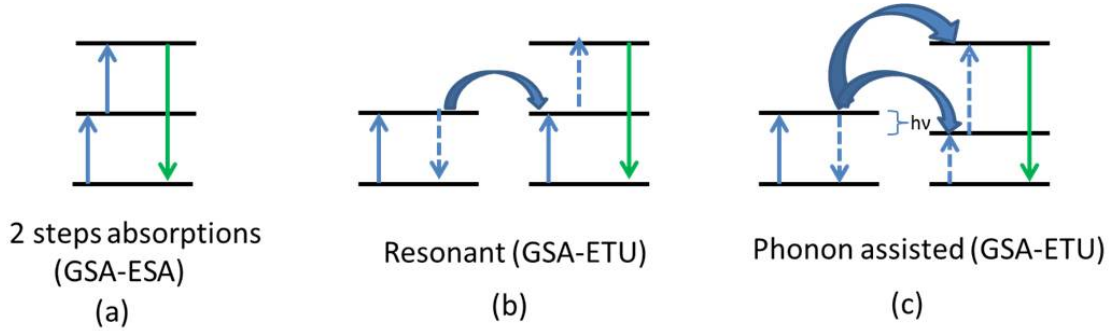
Figure 1.2: Upconversion mechanisms: (a) a two steps process where ground state absorption (GSA) and excited state absorption(ESA) occur in an ion and release a high enrgy photon (b) and (c) represent energy transfer upconversion (ETU) processes with resonant coupled and phonon assisted respectibvely.

n decreases and approaches to 1 at exteme pump power. A number of different mechanisms are involved in the upconversion process. Some of the mechanisms are depicted in fig 1.2. Figure 1.2 (a) is a process happens in a single ion when it absorbs two consecutive photons and excites an electron to the higher energy level with an intermediating level step. This process is also abbreviating as excited state absorption (ESA) and it demands a long life time of intermediate state. Figure 1.2(b) represents the resonant energy transfer upconversion (ETU) process where two ions participate. After absorption of each photon by the both ions, one releases its energy to the nearby ion and get de-excited to the ground state however makes other to excite electron to the higher energy state and luminescence of that ion gives a high energy photons. In general, ETU is dominant over other form of excitations in lanthanide by non-radiative transfer based on electric dipole-dipole interaction.This energy transfer rate (ETR) is strongly depends upon the inter-ion spacing, can be shown as:

$$ETR \propto \frac{1}{R^6} \qquad \text{: for dipoles,} \tag{1.2}$$

$$ETR \propto \frac{1}{R^8} \qquad \text{: for quadrupoles,} \tag{1.3}$$

This resonant ETU requirs energy overlap of intermediate energy level between both ions however no overlap give rise to have an assistance from phonons in order to occur this process call phonon assisted ETU as depidted in figure 1.2 (c). In this process phonons of energy equivalent to the difference between intermediate energy states ($h(\nu)$) of both ions can get generated or consumed to accomodate this ETU process.

ETU process can occur in same type of ions (Er ions) or different types of ions (Er^{3+} and Yb^{3+} ions) depending upon their matching energy states. The dominancy of one over other depends upon the chosen one or combination of two or three lanthenide ions.
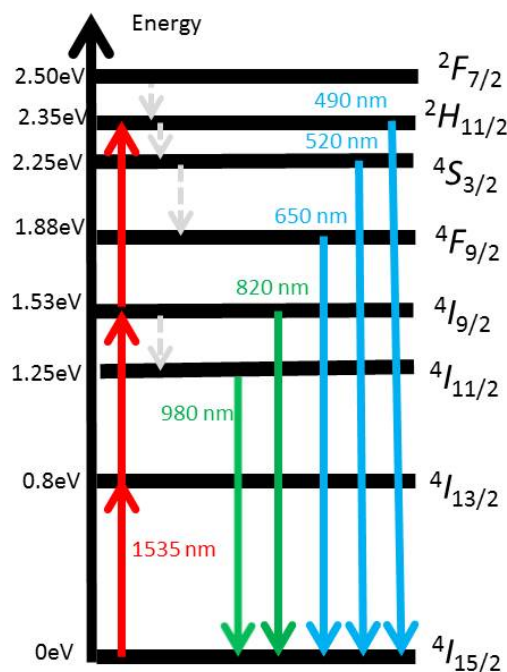
Figure 1.3: 4f energy level of Er^{3+}.The red, green and blue arrows show the excitation of 1535 nm wavelength, emission at NIR (980 nm and 810 nm),visible emissions respectively. The dash arrows show the possible non-radiative emission processes.

1.1.2   The lanthenides and the hosts

In this work, I deal with Er^{3+} ions as an emitter and both thin film (eg. TiO^2) and $NaYF_4$ nanostructures as hosts for this emitter.

Erbium

Er is an optical active lanthanide which show emission and absorption optical properties on a suitable light excitation. Suitability of the excitations depends upon the energy levels diagram of the participating shells. Erbium in ground state have electronic configuration $[Xe]6s^24f^{12}$ however on ionized trivalent state, its configuration becomes $[Xe]4f^{11}$. Due to this partly filled 4f energy state, Er^{3+} is more interesting material in upconversion process. The 4f energy level diagram of this ion can be seen in the figure 1.3.

After studying the emission levels of Er^{3+} ion, we can say that it is appropriate material for the crystalline-Si. Unfortunately, it has weak and narrow absorption and emission band makes it low efficient upconverting emitter.

TiO_2 *as a lanthanide host*

A crystalline TiO_2 has three phases; anatase, rutile and brookite. The rutile phase is more energetically stable than the other two. The doping of ions in to the TiO_2 host either replace the Ti^{4+} ions or sit on interstitial sites[18]. Independent of the occupant site, Er^{3+} ions will induce

lattice distortion in the host. This is due to the difference in ionic radii and charge. At high doping concentration,the crystal lattice get distorted and host become amorphous in phase[19]. I have chosen TiO_2 as a host for this emitter because of the several reasons. First, the phonon energy is very low in TiO_2 and that reduces the multi-phonon relaxation in Er^{3+} ions. Secondly, due to the high band gap, 3.2 eV, it is almost transparent to the visible spectrum range where Si absorbs and finally, it is a cheap material.

$NaYF_4$ nanocrystals as a lanthanide host

$NaYF_4$ is known as one of the most excellent host lattices for upconversion (UC) luminescence of the Er^{3+} ions, due to its low phonon energy,transparency over not only visible but also near infra-red (NIR) spectrum range and high chemical stability [21, 22]. The crystal structure of $NaYF_4$ exhibits two crystallographic forms, namely, α-cubic and β-hexagonal phases, depending on the fabrication method and synthesis conditions [20]. Previous research have shown that the β-hexagonal polymorph exhibits enhanced UC emissions compared with the α-cubic phase.The Er^{3+} doped β -$NaYF_4$ crystals have many advantages, including sharp emission peaks, large anti-Stokes shifts and long-lived excited electronic states [23, 24]. Therefore, β-hexagonal phase was an obvious choice for this work.

1.1.3   Plasmonics

In Drude free electron model, a metal is described as a material having free electron moving around a constant background of immobile ions. In general, electrons and ions are in equilibrium however any disturbance in electron density leads to setting up an electric field. As a result, electron oscillates and this is called as plasma oscillations. The quanta of these oscillations are called plasmons. The frequency of the plasmon is given by:

$$\omega_{(p)} = \sqrt{\frac{n_e \times e^2}{m^* \epsilon_0}} \tag{1.4}$$

Where n_e is the electron density, e is the charge of the electrons, m^* is the effective mass of the electron and ϵ_0 is the dielectric constant of the free space.

Depending upon where the electrons oscillate in material, the plasmons have different properties. The direction of oscillations of the plasmons is longitudinal. Due to the transverse polarization, light can not excite bulk plasmons [25]. The plasma oscillation at the interface of metal and dielectric called surface plasmon polaritons (SPP). SPPs are confined but can travel to few micron before get decayed[26]. SPP have both transverse and longitudinal electric fields and transverse component can interact with the light, however greater wave vector of SPP doesn't allow to excite with light[25, 26]. On the other hand, plasmons on the surface of the nanoparticles can interact with the light. They are called localized surface plasmons (LSP). LSPs are non-propagating waves (no wave vector) arise on the surface of the nanoparticles. Light can excite these plasmons due to its no wave vectors property [25, 26]. This is explained in the figure 1.4 (a). The electromagnetic (EM) wave disturbs the electrons slightly away from the equilibrium
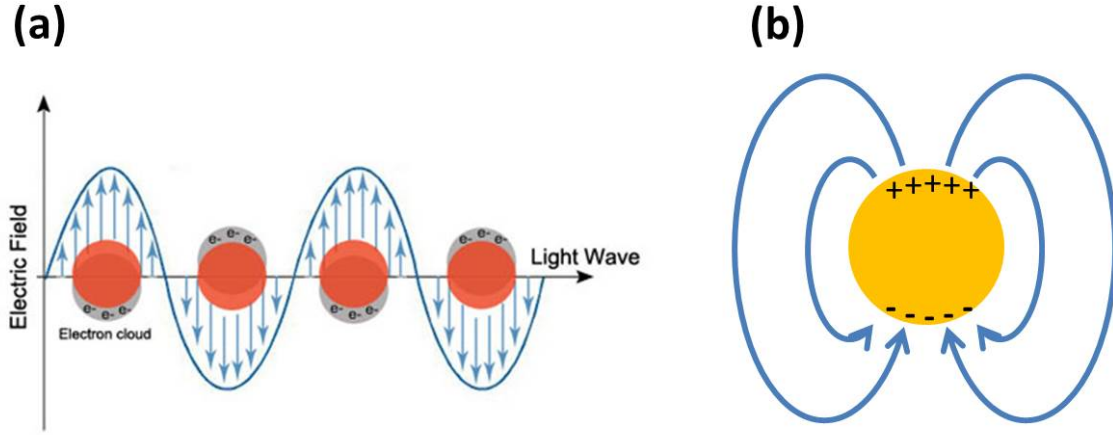
Figure 1.4: (a) an illustration of plasma oscillations in a metal sphere coupled to light. The displacement of the electron cloud results in an electric field generation. (b) strong localized near field around a metal particle after interaction with the EM wave

and that gives an electric field. The electrons acquire a momentum from the field and generates LSP. The restoring force drives the electrons at a specific frequency which is determined by the geometry of nanparticles, the effective mass of the electron and by the density of the electron. The oscillation frequency is called the plasmon resonance of the LSP. At resonance, a coupling between light and nanoparticles occurs and that amplifies the field outside (near-field) and inside the nanoparticles as shown as a sketch in figure 1.4(b). In case of a small uniform spherical metal particle where radius of sphere is a and that is very small compared to the wavelength of the electromagnetic wave (a<<λ). The EM wave can be assumed constant across the particle. Therefore that interaction of the particle with the EM wave can be treated by electrostatic approximation. The potential outside and inside the sphere can be calculated from Laplase equation ($\bigtriangledown^2\phi$=0). From this the dipole of the particle can be calculated:

$$p = 4\pi\epsilon_m \frac{\epsilon_{np} - \epsilon_m}{\epsilon_{np} + 2\epsilon_m} a^3 E_0, \tag{1.5}$$

Where E_0 is the uniform static electric field, p is dipole moment, a is radius , ϵ_{np} and ϵ_m are dielectric functions of the nanoparticle and the medium.

From here we can reach on the LSP resonance frequency dependence[25]:

$$\omega_{LSP} = \frac{\omega_p^2}{1 + 2\epsilon_m}, \tag{1.6}$$

If surrounding medium is considered 1 then LSP resonance for a small spherical particle can be written as:

$$\omega_{LSP} = \frac{\omega_p}{\sqrt{3}}, \tag{1.7}$$

Hence LSP resonance depends upon the electron density and the effective electron mass through ω_p.

1.2   Objectives

This work is a part of a project name 'High-efficiency solar cells by spectral transformation using nano-optical enhancement (SunTune)' which has been started to enhance the solar cells efficiency by mean of applying highly efficient upconverting and downshifting materials. In SUNTUNE, the upconversion process will be implemented onto the currently available solar cell platforms and ensure the efficient upconversion by introducing specially designed plasmonic nanostructures. My PhD study mainly focuses on an optimization of the upconverting materials by selecting appropriate host between thin film and nanostructures.

I have divided my objectives into three main sections where first two sections are currently running and initial findings have been achieved whereas the last objective have not been started yet but will be done soon. These sections are:

1. Here my main focus is on the study of plasmon enhanced upconversion of 1500 nm wavelength light in Er^{3+} doped TiO_2 thin film. In this work I answer some un-resolved issues: plasmon optimization at 1500 nm wavelength for efficient upconversion, a good agreement between experimental findings and simulation. So far, an upconversion enhancement has been achieved with specially designed Au nanostructures having a rather complex geometry. A finite element numerical approach validates the experimental measurement in a certain limit. The model lacking some of the parameters which needed to be included. Currently one of the PhD in our group is working in this direction.

2. In this section, I focus on $NaYF_4$ nanocrystals as a host lattices for Er^{3+} emitters and find the best approach to deposit Au nanostructures close to the emitters which gives a efficient enhancement at 1500 nm wavelength. The upconversion enhancement will then be compared with the TiO_2 thin films in order to find the best host and the best position for the specially designed Au plasmonic structures in the Er^{3+} environment. I have divided this work further into two sub-sections where in first section I deposit optimized Au nanodiscs on top of a thin film of commercial $NaYF_4$ nanocrystals and in second section, I chemically link the commercial Au nanorods (designed for 1500 nm plasmon resonance) with the $NaYF_4$ nanocrystals by a neck-formation strategy and then make a thin film of this via drop cast assisted spin coat technique. So far, I have optimized a way to coat a chemically and thermally stable, almost crack-free thin film of Er^{3+} doped core-shell TiO_2 nanocrystals. The optimized Au nano-discs have also been placed successfully. In addition, the second sub-section still requires some more work to obtain a mixed thin film. The preliminary findings are reported in the relevant chapters of this report.

3. Implementation of an enhanced upconverting thin film into the currently available Si-bifacial solar cells and study the influence of upconversion on the photo-voltaic conversion efficiency will be done.

Chapter 2

Experimental Techniques

The list of the techniques involved in my work are reported below:

1. Fabrication techniques-RF-Magnetron Sputtering (RF-MS), Electron Beam Lithography (EBL) and Spin Coat

2. Techniques for structural and optical characterizations- Electron Microscopes (Transmission Electron Microscope (TEM) and scanning Electron Microscope(SEM)), Ellipsometry, Spectrophotometry, and Photo Luminescence (PL) .

In this section I present the two main techniques where I was heavily involved. The descriptions are briefly written.

2.1 Radio frequency magnetron sputtering

The studied upconverter Er^{3+} doped TiO_2 has been fabricated by this technique. The upconversion luminiescence (UCL) of the samples is optimized to yield highest efficiency by changing the deposition parameters of the RF-MS technique.

This plasma assisted technique is used for thin film deposition as shown in figure 2.1 (a). The plasma is generated by an introduction of Ar (noble gas) gas in a vacuum chamber containing two electrodes. On applying electric field on the electrodes, stray electrons accelerates and creates electron-ion pair (e^--Ar^+), that leads to a plasma in the chamber. As the technique name suggests, the applied voltage is an alternating voltage which periodically reverses direction at a frequency of 13.56 MHz. Due to the pulsating field, stray electrons might get additional energy from the alternating field and that makes easy formation of plasma. RF-MS has advantage over DC- MS (direct current-MS) because of easier ionization and ability to produce high quality oxide layer [27].

When the plasma is stabilized, essentially all surfaces in the vacuum chamber are negatively charged. Due to the light weight, electron mobility is higher than the Ar^+ ions and this gives the negative charge to the surfaces. Therefore the periodic change of the electric field is felt more by electrons than ions. The negativity of the target is more than the positivity of the substrate due to the high electron collision probability than the ions.This makes the target more negative due to more electron collision as compare to the collision of the ions to the substrate to get more positive. Now the target is negative and it attracts more Ar^+) ions. This positive ion bombardment eventually eject atoms from the target. The sputtered atoms pass through the plasma and get deposit on the substrate, one atom at a time resulting in a thin film. The magnets below the target keep the plasma nearby.

Once the single atom get deposited to the substrate the chance of deposition of another atom
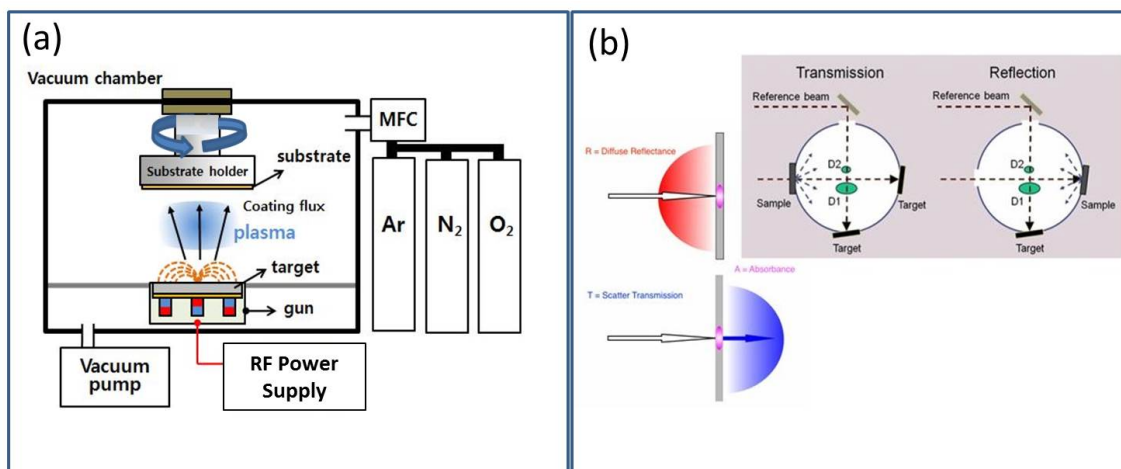
Figure 2.1: (a) schematic representation of a rf-sputtering system. (b) depicts the optical diagram for both the reflection and transmission measurements of the double beam integrating sphere.

increases and then nucleation makes a small island. The island grows till its critical limits and then this island formation spreads over the surface. This nucleation process leads to the lateral and perpendicular growth of the nuclei. The lateral growth results in the continuous film by connecting islands whereas the perpendicular growth later works on the film thickness.

2.2 Spectrophotometery

The spectral wavelength of the plasmon resonance of Au nanostructures is obtained from spectrophotometer by calculating extinction energy from transmission and reflection measurements. The resonance occurs when electrons oscillate with the incoming photons, results in scattering and absorption of the incoming light.

The spectrophotometer used for this study is a Lambda 1050 instrument from Perkin Elmer equipped with 150 mm integrating sphere to collect all the scattered light from the nanostructures. The instrument scan in range of 175 nm to 3300 nm. However so far I worked in 300-2500 nm range for this work. The sphere has several openings and one in front is for total transmittance (TT) and one at the back is for the total reflectance (TR) as shown in the figure 2.1(b). The total word in both TT and TR stands for the inclusion of direct and scattered light. The sample is angled $8°$ with respect to the incoming light, to prevent specular reflected light . The transmission measurement also performed on $8°$ angle to match the reflection.

Chapter 3

Plasmon enhanced upconversion of 1500 nm wavelength via Er^{3+} doped in a TiO_2 matrix

This work has been written for APL peer-reviewed research journal and will be submitted shortly. This chapter has a combined experimental-simulation study of Au nanostructures enhanced upconversion in Er^{3+} doped TiO_2 matrix. The major contributions of others in this work are: The Au deposition by Dr. Adnan Nazir, a post doctoral fellow in our group, the simulation study by Assoc. Prof. Søren P. Madsen and upconversion measurement by Jeppe Christiansen, a PhD in our group. I have mainly contributed in sample fabrication, in all structural and some optical characterizations and in complete manuscript preparation.

3.1 Aim

Plasmonic enhancement of upconversion process at 1500 nm wavelength is poorly reported. Therefore, there is a strong need to explore this issue. J. Goldschmidt et al. [13, 14] have reported a simulation study using a simple spherical geometry of a plasmon. However, near field is more enhanced in the presence of sharp edges in a plasmonic nanostructure compared to a complete lack of edges[15]. Therefore, a study of the complex geometries of plasmonic nanostructures is required to gather realistic information on the potential for enhancement of upconversion efficiency at the 1500 nm wavelength as well as for controlling the configuration of nanostructures to achieve the said efficiency. In this work, we have chosen a truncated cone shape for Au nanostructures. The engineering of these nanostructures was defined with a finite element modelling (FEM) and experimentally realized afterwards with electron beam lithography (EBL). An enhanced upconversion luminescence have been achieved with these nano-structures. The FEM shows a good agreement in a certain limit to the extinctions and the luminescence measurements.

3.2 Sample fabrication

A 100 nm thick Er^{3+} doped TiO_2 samples were prepared by radio-frequency magnetron-sputtering (RF-MS) technique on fused quartz substrates. During sputtering, the substrate temperature was 355 °C with 100 W RF power and 0.4 Pa gaseous environment (2 % O_2 in Ar atmosphere)inside the chamber. The sputtering target contained 5.1 at% Er^{3+} in TiO_2. The EBL defined Au discs were placed on the top of the upconverting film in a way that both measurements with and without of these structures could be performed on one sample.
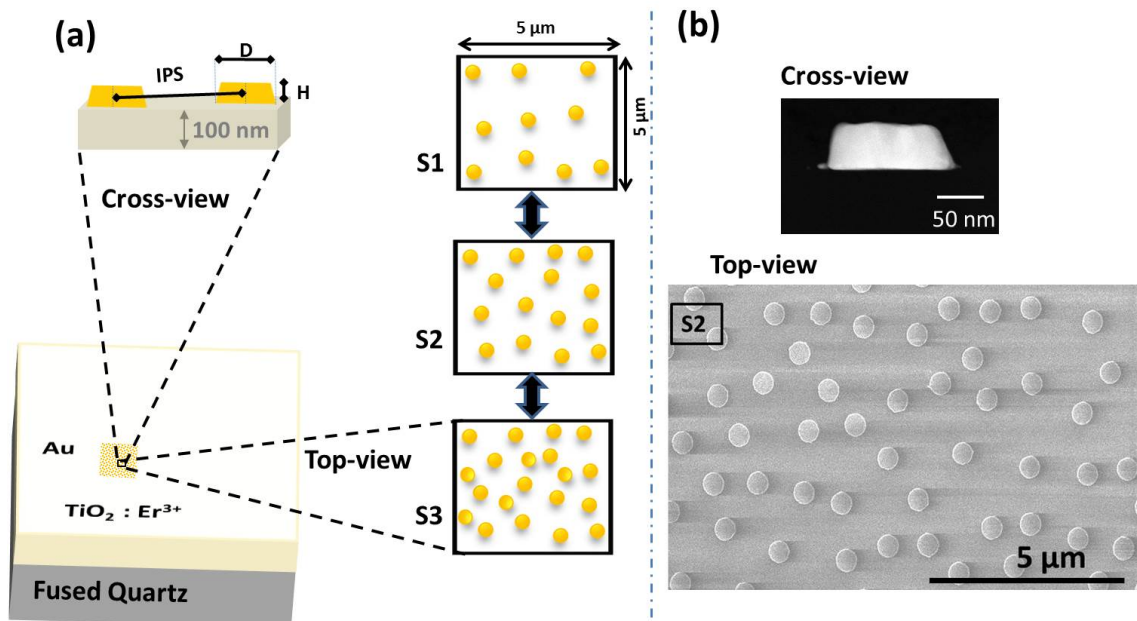
Figure 3.1: Schematic and experimental realization of fabricated samples (a)sketch representation of 3D-view, top-view, andcross-view of samples. The top-view shows 3 different sets intented to depict the particle density and distribution over a imagined (5×5 μm^2) area of total fabricated area which is 2×2 mm^2 represented on 3D-view. The cross-view indicates the geometric parameters: the height as H, the diameter as D and the interparticle spacing as IPS of fabricated Au nano-discs. (b) the scanning electron micrograph of top-view and cross-view of two random samples. The top-view shows a sample with H=50 nm, D= 480 nm of the set S2 whereas cross-view is a Au nano-disc with D= 147 nm.

3.3 Results and discussions

This reduces the sensitivity to variation in sample fabrication. The structure of samples is presented in figure 3.1(a) and scanning electron microscope (SEM)image of one of the fabricated samples is in figure 3.1(b). Three sets of samples with a variation in particle density has been sketched. However, the introduction on these samples is described later in this chapter. The SEM image shows the random spatial distribution and the homogeneity in shape and size of experimentally realized Au discs. The fabrication of the Au discs were guided by a numerical model, FEM, which solves the Maxwell equations and gives the optimal geometric parameters for the fabrication.

The model computes the field distribution around a single particle over a range of wavelength in a definite domain where boundary is kept non-interactive with the reflective waves by introducing perfectly matched layer around the domain [28]. The model does calculation after taking the refractive indices of all the layers involved in the model. In this calculation, the tabulated refractive indices of Au [29] and quartz [30] have been taken whereas refractive index of Er doped TiO $_2$ were measured by ellipsometry. The simulation has taken the truncated cone as a shape for the Au structures with 1.1 times bottom to top radius. The diameter and height of the structures were varied from 200 nm to 600 nm and 10 nm to 100 nm, respectively, with

(a)

(b)
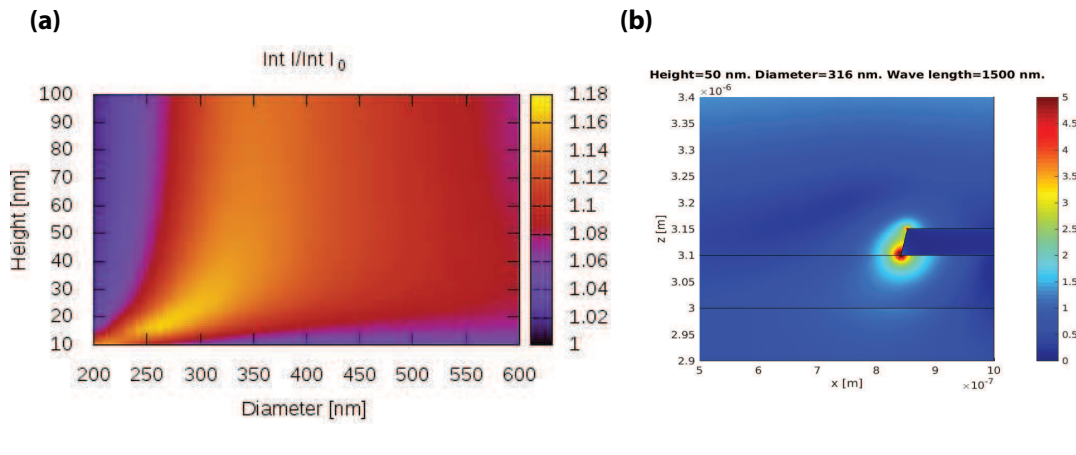
Figure 3.2: (a)Integrated intensity FEM calculation over a range of geometric parameters of Au discs with incoming light at 1500 nm wavelength at normal incidence. The color bar indicates the intensity enhancement.(b)An electric field distribution around an optimized Au nanodisc which is on 100 nm TiO_2 film at 1525 nm wavelength illumination.

steps of 0.5 nm in the scan. The enhancement in intensity has been calculated as:

$$L^{(n)} = \frac{\int_{V_{UC}} I^n dV}{\int_{V_{UC}} I_0^n dV},$$ (3.1)

where V_{UC} represents the volume of the upconverting layer, n represents the number of the photon requires to populate the emission level, I and I_0 are the intensity with and without nanoparticles respectively. In this experiment, we expect to have n=2 for a strong emission at 980 nm when the Er^{3+} get excited with 1500 nm wavelength. However, at some point the upper levels become saturated due to high lasers pump power, and that leads to a decrease in n value. At very high pump power, saturation approaches and n becomes 1. The upconversion efficiency can be optimized by selecting the geometric parameters corresponding to the highest value of L. The simulated result are plotted in figure 3.2 where 3.2(a) shows the intensity enhancement at n=1, $L^{(1)}$ corresponding to a saturation level. The simulation provides highest enhancement at height below 20 nm with in range of 250 to 300 nm in diameter. Due to the wide acceptance region in diameter at height 50 nm, the experiment were performed on the same height. Figure 3.2(b) shows us the electric field distribution around the nano-disc which is on top of the 100 nm thick Er^{3+} doped TiO_2 layer. Just for the clarity an exact half portion of a disc has been depicted in the figure. The enhancement of the electric field around the disc can easily be interpreted. At a 50 nm constant height, the field enhancement lies over a complete scanned diameter range therefore a set of the samples with diameter from 150 nm to 600 nm has been chosen to fabricate.In order to investigate the effect of the inter-particle interaction we have designed 2 more sets with different particle-particle distance by varying the particle density (PD) during EBL process. The concentration of particles were kept 4000 per unit 100×100 μm^2 area in one set and increased to 6000 and to 8000 in other two sets. Due to the chance of geometric shape distortion from nearby particles during fabrication with EBL, called proximity effect, the concentration above 8000 was not possible in the defined area. All 9 patches of differnt sized Au nano-structures from each set were fabricated on a single 3×3 cm^2 quartz substrate

which reduces the effect of sample variation. To avoid enormous text, S1 is abbreviated for samples with PD 4000, S2 for PD 6000 and S3 for PD 8000. For example, sample with 6000 PD and a 315 nm diameter is called as sample S2-D315 throughout the paper and so on.

The 150 mm InGaAs integrated sphere spectrophotometer has been used to perform direct transmittance (T$_D$) and direct reflectance (R$_D$) measurements in a wide spectral range. The extinction cross section, σ_E, has been calculated from the above two terms as:

$$\sigma_E = \frac{1 - T_D - R_D}{PD} \tag{3.2}$$

. In figure 3.3(a), the extinction cross section per disc area ($\frac{\sigma_E}{A}$) as a function of energy (E) and corresponding wavelength ($\frac{hc}{E}$) is shown for samples where SPR spectral peak of Au nano-discs is either at 1500 nm wavelength or closest to it in each set. The experimental findings have been compared with FEM predictions as shown in this figure. The experimental results of $\frac{\sigma_E}{A}$ had some high frequency noise and background noise therefore further smoothening were performed by Percentile filter and Savitzky-Golay filter respectively in origin software. These filtering tools remove the unwanted noise leaving behind the actual spectra. The experimental and simulation data show several orders of SPR spectral peaks where the first order SPRs are in visible range and the desired second order peaks are in near infra-red (NIR) spectral range.The finite element simulation has shown the SPR peak position at 1500 nm wavelength for the sample with diameter 315 nm. However, experimentally we couldn't realize the same diameter for S2 and S3 sets. Therefore, in the figure, comparison has been made with some sample having diameter close to the 315 nm (FEM defined which gives SPR at 1500 nm wavelength) but not the exact. Most interestingly, we see the two resonance peaks in S1-D315 sample in the NIR region at E=0.82 eV which could be a result of Au-Au nano-discs interactions. On further understanding about this inter-particles interaction, the figure 3.3(b) has been plotted to show the generation and the extinction of this two peak system with variation in discs size in set S2. The plots are vertically shifted for the clarity purpose. In the figure,the first peak at E=1.20eV is dominant over the second peak which is at E=0.74eV in sample S2-D308 however it gets recessive as we increase diameter and further increase results in a single peak in sample S2-D380.

In order to see the overall trend of the experimental data of all the samples in-comparison to the simulations figure 3.3 (c) has been plotted. Here we see a good agreement of data values with the simulation and a dependence of the energy position of the two-peaks system on the inter-particle spacing. This two-peaks system can be considered as a collective oscillation of a dipole with the neighboring dipoles which may consider as a inter-particle coupling effect. The inter-particle spacings has been calculated by taking mean of center-to-center distance of four nearest particles and the value were around 1680 nm for S1, 1280 nm for S2 and 1180 nm for S3 samples. Zoric et. al. [16] have discussed in their work about the minimization of this effect in random array of nano structures by having center-to- center distance 6 times higher than the nano-disc diameter. According to Zoric's report, our system where desired diameter is 315 nm, the minimum particle-particle spacing should be around 1890 nm which may give around 3000
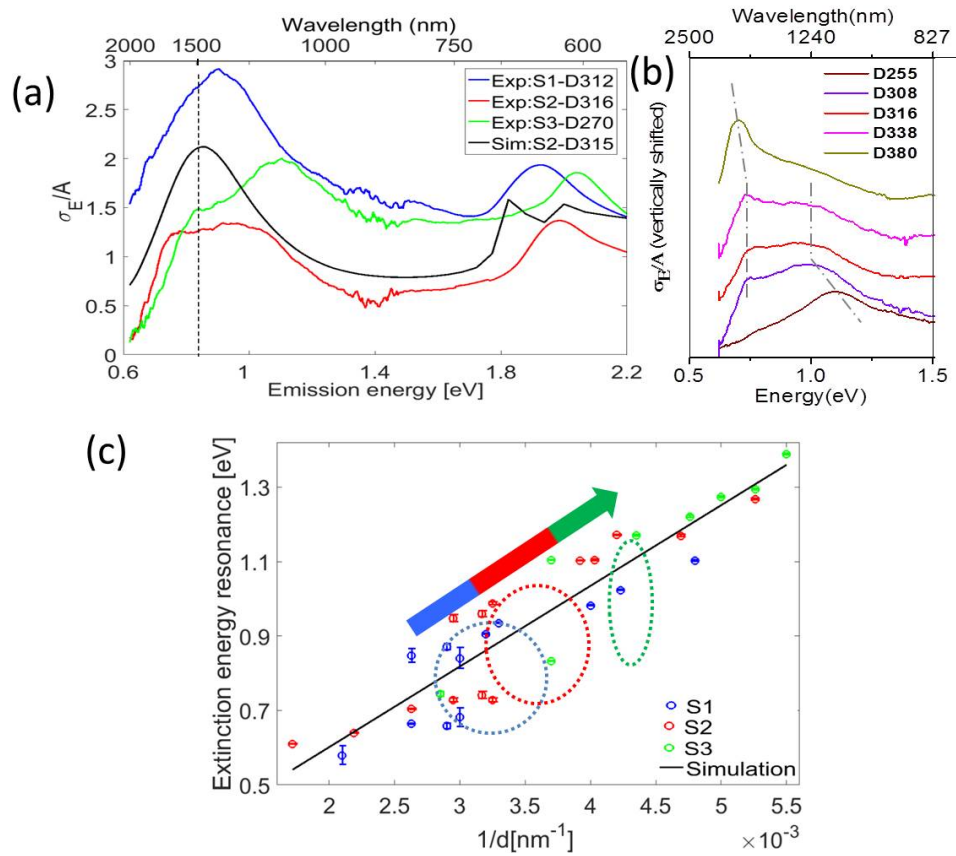
Figure 3.3: A variation in extinction cross section per disc area with the emission energy and its corresponding wavelength. A comparison between a simulation (315 nm diameter) and experimental data of one sample with SPR peak closest to 1500 nm wavelength of each set. The dash line indicates the excitation energy. (b) A variation in SPR peak position with diameter in set-S2. The generation and extinction sweep of two SPR peaks with variation in disc diameter. The two curved-dash lines depict the SPR peak position of a sample. (c)Scaling of extinction energy resonance with inverse nanodisc diameter.The discrete symbols correspond to experimental data points and black solid line is FEM calculation. The dashed circles show the inter-particle interaction and the arrow shows a shift in this with the particle density.

PD. Although may be the inter-particle coupling probably be shifted to the higher wavelength on this PD=3000 but low signal to noise ratio would not allow to observe the SPR peak at all in our spectrophotometer.

The upconversion luminescence spectra (UCL) spectra were collected under illumination of a continuous 1503 nm wavelength monochromatic laser with up to 22.9 mW power. The set-up to perform this UCL experiment consisted a spectrometer coupled with a CCD array for capturing the emitted light.In figure 3.4(a) the upconverted light intensity has been plotted as a function of wavelength. In this spectrum a Er^{3+} doped TiO_2 sample D315 shows a characteristic strong emission peak at 980 nm and this may involve the most efficient Förster resonant energy transfer (ETU) upconversion process. ETU is a process involves two nearby ions ; one ion relaxes by transferring its gained energy to the nearby ion and this ion then reaches an excited state. The two rather weak peaks at 660 nm and 550-525 nm result from $^4F_{9/2}$ and $^4S_{3/2}$- $^2H_{11/2}$ respectively to the ground state $^4I_{15/2}$.The place where nanostructures were defined gives more UCL at all
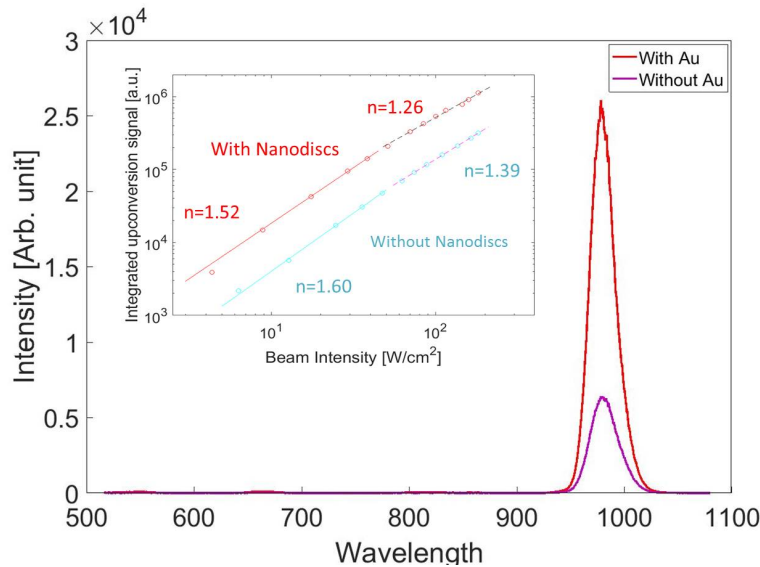
Figure 3.4: Photo-luminescence (PL) measurement in TiO_2:Er^{3+} with and without Au discs of sample D315 of set S2 while excited with 1503 nm monochromatic laser.(a) one spectral emission line for with and without Au disc regions. The upconversion enhancement occurs at all the possible emission energy levels.(b) UCL intensity as a function of pump power intensity in with and without nanodiscs in sample D315 from set S2. The data points correspond to 980 nm emission line. The least square fits give the exponents which correspond to the shown n values. A separate fitting is performed at high and lower bem intensity.

the emission peaks as shown in the figure 3.4(a). The UCL enhancement is higher at 980 nm wavelength emission than at other two emissions due to the high probability of consecutive 2-photons over consecutive 3-photons absorption process. However the consecutive 2-photons absorption also gives peak at 810 nm but multi-phonon relaxation ,an non-radiative emission, makes it less probable.

The power dependence measurements have been carried out to understand the saturation level on the working pumping power regime on both with and without Au discs area of a sample S2-D315 in figure 3.4(b). The figure shows the n= 1.60 and n=1.39 at low and high beam intensity respectively for emission peak at 980 nm on without Au disc area. On the contrary, the slope of all the samples decreased to n= 1.52 and 1.26 for the same when excitation took place at Au discs surface. The strong electric field around the Au discs as shown in figure 2(b) to the Er^{3+} ions might be a reason of this saturation in first excited energy level $^4I_{13/2}$. The value of n is lower than 2 indicates the saturation level. Therefore the FEM calculations for UCL enhancement should be with $L^{(1.5)}$ and $L^{(1)}$ in order to compare with experimental results.

In figure 3.5 shows the experimental together with simulations of $L^{(1.5)}$ and $L^{(1)}$ data for UCL enhancement in 980 nm emission peak as a function of nanodisc diameter. The experimental results of sets S2 and S3 show a similar trend of $L^{(1.5)}$ simulations. However set S1 does not follow the trend but shows a same level of enhancement. The experiments were carried out within an integrated sphere in order to have an absolute measurements of the emitted light. We found a largest enhancement of 980 nm emitted light for S2-D316 which is around factor of 7. However this experimental enhancement is 3 times more than the enhancement suggested by
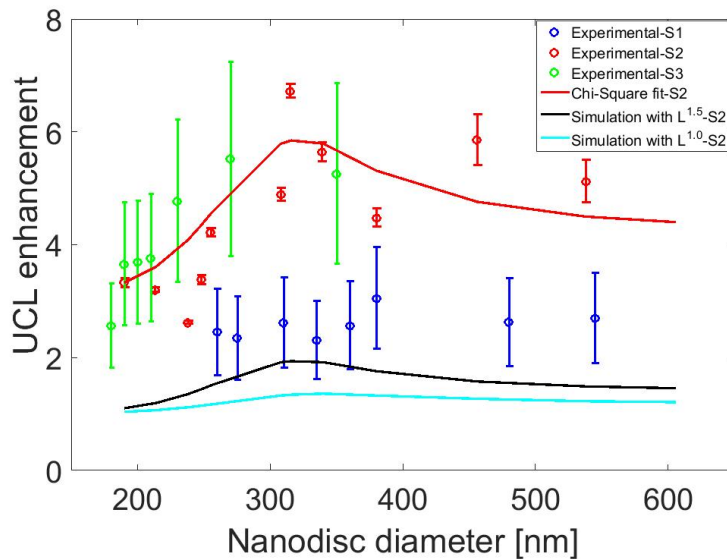
Figure 3.5: Scaling of the UCL enhancement at excitation energy 0.827 eV with the nanodisc diameter. The simulation at n =1.5 and 1 are compared with the experimental results of sets S1, S2 and S3 in the entire range of the disc's size. The width of the SPR spectral peak has given the error bars in the experimental results. A chi-square fit is drawn for the data points of set S2

$L^{(1.5)}$ simulations. The quantitative disagreement could be a reason of scattering phenomenon which is more dominant in nanoparticles with diameter greater than 200 nm. From this work we have demonstrated a true need for a fine model of plasmon fabrication which stands valid for a long range of nano structures and FE modeling could be a good option if it can be refined further. This model has already been successfully used for the 810 nm excitation wavelength [9].However it is first time we show this model for 1500 nm wavelength excitation over a range of large nano structures.

An advanced model should be designed with least 2 particle in a defined domain with 3-D scan by introducing IPS as another scan variable with height and diameter. The refined model should address inter-particle interactions, effect of particle-film interference and light scattering phenomenons. The current model consider the equal field enhancement for all the Er^{3+} in the film. However the distribution of electric field depends upon the vertical distance so the Er^{3+} ions far from the plasmons are unaffected. Therefore FE simulation with rate equation models could be a solution to this obstacle [31].

An absolute external power conversion efficiency (EQLE) has also been measured for all the samples of all three sets on both with and without nanodiscs. We have also used the integrated sphere for this measurements and the value of this EQLE is calculated by taking a ratio of the emitted power to the incoming power $\frac{P_{em}}{P_{in}}$. The data value of $EQLE_{without}$ and $EQLE_{with}$ were on-average 1.0×10^{-6} and in range of $2.0\text{-}5.0 \times 10^{-6}$ respectively for all the samples. The variation ($2.0\text{-}5.0 \times 10^{-6}$) in EQLE with nano-structure was because of the dependency over

the Au density. We have calculated 2-6 times enhancement in EQLE. This efficiency is rather low even though it has plasmonic enhancement. However this efficiency is more than 100 times higher than the previous report with same model where excitation was at 808 nm wavelength at Ag nano particles in Johannsen et. all.[9].

3.4   Conclusion

All in all, a plasmonically enhanced UCL in Er^{3+} doped TiO $_2$ thin film targeted at 1500 nm wavelength excitation has been demonstrated.The report reveals the variation in SPR spectral peak position with geometric parameters and the role of IPS on inter-particle coupling . The finite element modelling shows a reasonable agreement with the experimental findings over a full range of Au diameter. The experiment approves the feasibility of FE simulation in optimizing the geometric parameters this complex geometry of Au structures. The highest UCL enhancement is found in sample S2-D316 which is almost 7 times. However an advanced FE model for an exact agreement with experimental findings is needed.

3.5   Future work

So far, I have achieved plasmonically enhanced upconversion while placing Au nano-discs on top of the Er^{3+} doped TiO $_2$ thin film. will the UCL be affected if the Au nano-discs are buried into the thin film instead placing on top ？ The answer of this question will be resolved in this future work. Figure 2(b) of the current work, gives a nearly homogeneous field distribution around the nano-structures, however the current setup only able to absorb the field accumulated below the structures. Therefore, by placing Er^{3+} ions on above, on below and next to the Au nanostructures might capture all the field which is being non-captured in my present experiment. However, changing the sample structure would change the simulation and hence electric field distribution around the structure but that would not change the homogeneity in the distribution, I suppose. In this work I will make a setup where Au plasmons will be placed between the two Er^{3+} doped TiO $_2$ film as a sandwich structure. The plasmon structures will be optimized for 1500 nm wavelength excitation with the advanced FEM (Emil, a phd in our group, is working on the advancement in current FE simulation). The thickness of the top and bottom upconverting layer will be varied in order to achieve the highest UCL.

Chapter 4

Plasmon enhanced upconversion of 1500 nm wavelength via Er^{3+} doped in a $NaYF_4$ matrix

This work has not been finished yet and it is under-process. This chapter has only experimental findings of Au nanostructures enhanced upconversion in Er^{3+} doped $NaYF_4$ process. Dr. Adnan Nazir and Jeppe Christiansen are the candidates who have also contributed in this work. Adnan has deposited Au nano-discs on top of the film and Jeppe has performed UCL measurements for the film. I have mainly contributed in sample fabrication and in all structural and some optical characterizations. The chapter has been divided into two sections. The section 1 has report about the plasmon enhanced UCL of samples where EBL defined Au nano-discs are placed on top of the Er^{3+} doped $NaYF_4$ thin film. Whereas section 2 contains the information about plasmon enhanced UCL of a setup where commercial Au nanorods (SPR at 1500 nm wavelength) are chemically linked with Er^{3+} doped $NaYF_4$ nanostructures and thin film of this mixed-nanostructures is coated afterwards.

4.1   SECTION-I

4.1.1   Sample fabrication

A commercially available 20-5 nm size core-shell Er^{3+}: $NaYF_4$ - $NaYF_4$ structures have been used as a upconverting medium for this task. The film has been coated on a quartz substrate via drop-cast assisted spin coat technique, a technique where a drop of a nanoparticles solution is spin-coated directly. The spin speed was set to 3500 rpm for 40 sec time span. The post heat treatment of the film has been performed at $100\,°C$ in an regular oven. The chemical stability of the film has been verified via treating with Acetone. The EBL defined Au discs were placed on top of the optimized upconverting film in a way that both measurements with and without of these structures can be performed on one sample. This reduces the sensitivity to a variation in the sample fabrication.

4.1.2   Preliminary results and discussions

The SEM micrographs of samples are presented in the figure 4.1. The thickness of the film was optimized to 160 nm with an error of 20 nm. The top view image in the figure 4.1 (a) gives the homogeneity in distribution and shows the presence of nano-cracks in the film whereas the cross section view in the figure 4.1(b) gives the qualitative roughness of the deposited film. Regarding
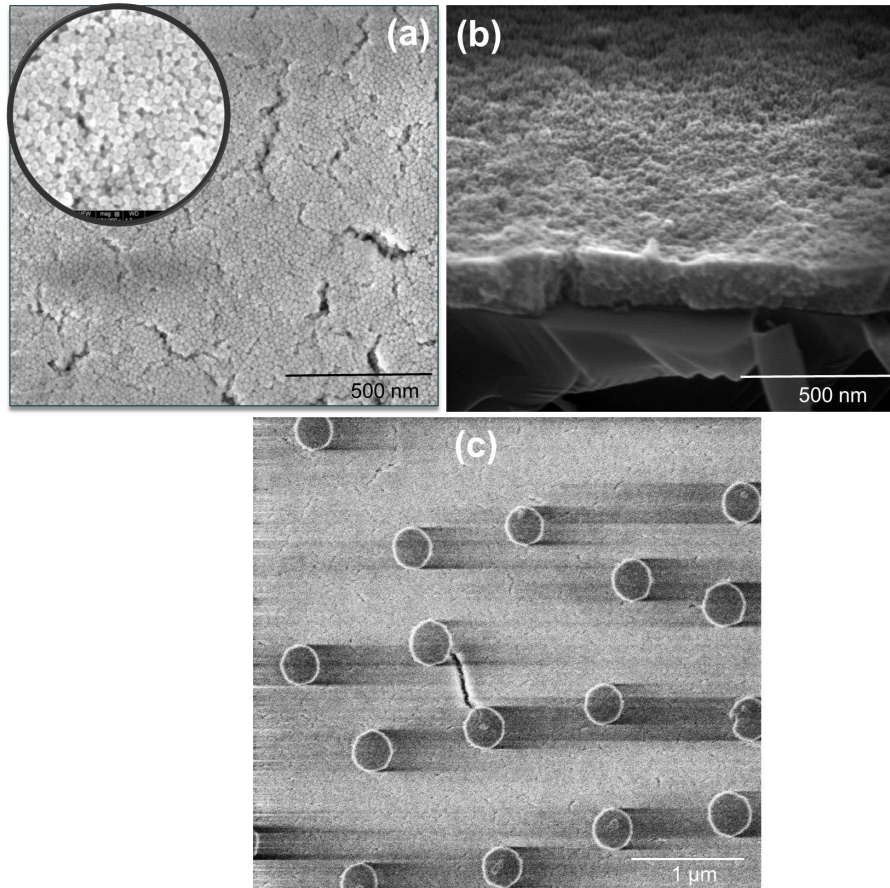
Figure 4.1: SEM images (a) the top view of drop cast assisted spin coated Er^{3+} doped $NaYF_4$ thin film on quartz substrate. The inset is a magnified image of the same. (b) The cross section view of the film deposited on the Si substrate. The trashes of Si substrate can be visualized in lower portion in the figure. (c) the top view of EBL defined Au on Er^{3+} doped $NaYF_4$ thin film. The dimensions of nano-discs are: 310 +10 nm diameter and 50 nm height.

the upconversion enhancement Au nano-discs are placed on top of the film via EBL process. During EBL, film faces acetone like harsh chemical. Therefore it is important to have thermally and chemically stable film. However on the same time the cracks and the roughness in the films are also hurdles for the EBL process to execute the exactly same simulation-defined Au nano-discs. A crack-free surface can be obtained by excluding the post-heating process (SEM images are not included in the report) but then chemical stability is no longer the part of this. Several repetitive experiments with uniform and non-uniform heating have given the good understanding of optimal heating parameters. The heating from hot plates gives more cracks on the film at a temperature where chemical stability meets. In this non-uniform heating, solvent (toluene) evaporates instantly which develops major cracks on the surface. The 100 °C temperature in an uniform heating environment (by an oven) has given the optimized thin film. These films were chemically stable and the cracks were in nanometer scale. A random array of Au nan-discs with 310+10 nm diameter and 50 nm height has been defined by EBL technique on the optimized thin film. The defined structures can be seen in the figure 4.1(c).

Some preliminary optical measurements are performed on the obtained thin film. In figure 4.2
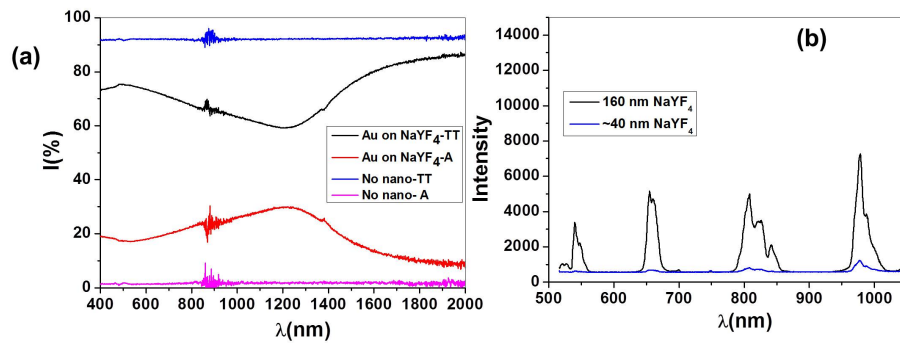
Figure 4.2: Optical measurements (a) transmission and absorption measurements of the samples with and without Au nano-discs deposited on Er^{3+} doped $NaYF_4$ thin film. TT and A are the abbreviations for total transmittance and absorption respectively (b) UCL measurements of Er^{3+} doped $NaYF_4$ thin film with different thickness.

(a), an around zero absorption over a complete wavelength range has been achieved for the film without Au nanostructures . The SPR peak position was obtained at 1260 nm for a sample with 310 nm diameter. The results for 1500 nm SPR will be presented after getting inputs from the simulations. The UCL measurement has been performed with 1500 nm wavelength excitation and emissions have been plotted in figure 4.2(b). The emissions at 980, 810, 660 and 550 nm wavelength have been obtained. The thickness of the film has been reduced further to see the effect on the UCL and also the feasibility of the AU deposition process. However the Au has not been deposited on 40 nm Er^{3+} doped $NaYF_4$ thin film. UCL measurement with the Au nano-discs are under-process.

4.1.3   Future works

Future work has been devided for the two main objectives. First, An advanced FEM simulation will be developed for this setup to get an optimal input parameters for Au plasmons for resonance at 1500 nm wavelength. This Au assisted structure will be tested for the UCL measurements. The role of IPS will be determined, if necessary. Second, An upconversion enhancement will be acquired with different thicknesses of the film for different purposes: 1. A lowest thickness (eg. monolayer) with an observable UCL will be achieved for the deposition of EBL defined Au plasmon . This will give an insight about the particle level interactions. 2. A 100 nm thin film will be fabricated for a comparison with results from chapter 3 while keeping the constant dopant (Er^{3+} ions) concentration.

4.2   SECTION-II

In this Au linked UCNP (upconverting nanoparticle) film, I expect to have a higher degree of upconversion enhancement than placing Au on top of the film. In this film, I expect to have
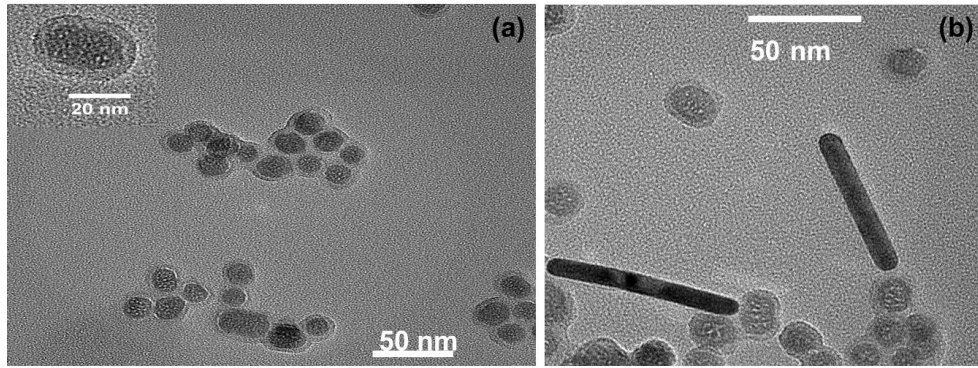
Figure 4.3: Transmission electron microscope (TEM) images (a) NH^{2+} grafted SiO_2 capped core-shell Er^{3+}: $NaYF_4$ - $NaYF_4$ structures. The inset shows the single particle with a clear 5 nm thick SiO_2 cap (b) Au linked-$NaYF_4$ structures.

a high degree of upconversion enhancement due to the nearly equivalent local field distribution around all the Er^{3+} emitters.

4.2.1 Sample fabrication

In this process, so far the same UCNP structures are used which are defined in section 1 of this chapter. In a well-reported procedure [32], 0.8 mL of Igepal CO-520 (NP-5) was dispersed in 17 mL of cyclohexane and stirred it for 30 minutes. Afterwards, 0.15 mmol UCNP-cyclohexane solution was injected into the mixture. After magnetic stirring for 3 h, 0.14 mL of ammonia (25 percent) was added. The flask was sealed and stirred further for 10 minutes. Using a Syringe Pump to control the adding rate, 0.075 mL of TEOS (Tetra Ethyl Ortho Silicate) was added with 1 mlh^{-1} rate into the system to get controllable thickness of silica 5 nm. The mixture was sealed and kept stirring for 24 h. To graft amino-groups, 30 mL APTES (Amino Propyl Tri-ethoxy Silane) was injected into the system and kept stirring for 4 h. Methanol was then added to precipitate the product. Collected by centrifugation, washed with ethanol several times, the product was finally dispersed in ethanol. Mixing UCNP@SiO2-NH2 with Au nanorods solutions together, the Au nanorods could be attached onto the silica surface after 20 min of ultrasonication.

4.2.2 Preliminary results and discussions

The SPR peak position of commercial Au nanorods is at 1450 nm wavelength however the peak is 150 nm wide and has a tail at 1500 nm wavelength. The figure 4.3 shows the TEM images where (a) shows the only SiO_2 capped UCNP and (b) shows Au nanorods linked with thse UCNP. The capping thickness is a function of the TEOS precursor concentration. The energy transfer from Er^{3+} back to Au has been reported therefore it is important to have dielectric spacing between Er^{3+} ions and Au plasmons [13]. Several experiments have been performed on Er^{3+} doped $NaYF_4$ in order to find the optimum dielectric spacing. Sabokttakin et. al. [33]
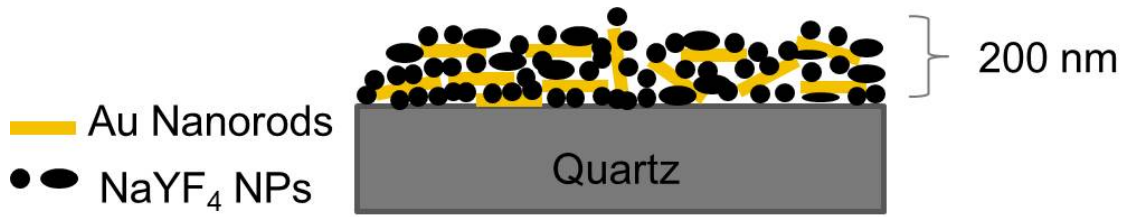
Figure 4.4: Schematic representation of the mixed (Au-UCNP) thin film.

have found 10 nm spacer as optimum for UCL enhancement. Therefore 10 nm has been defined for the present experiment where 5 nm is SiO_2 and rest 5 nm is the thickness of shell of the UCNP.

4.2.3 Future works

A thin film will be deposited of this mixed nanoparticles via the spin coat technique as shown in figure 4.4 and UCL and extinction energy measurements will be carried out further. However, the multi-directional deposition of the Au nanorods in the film will affect the plasmonic properties of the rods and might not give any UCL enhancement. Therefore, an additional approach will be implemented to get directional deposition of Au rods in a nano-patterned substrate. The pattern on the substrate can be developed by depositing a PDMS mold with nano-patterns and that will guide the rods during deposition[34].

Chapter 5

Summary and Outlook

5.1 Summary

To summarize:

1. Plasmonically enhanced upconversion of 1500 nm wavelength light has been obtained in a Er^{3+} doped TiO_2 system. A combined experimental-simulation study has been presented for a random array of truncated cone shaped Au nanostructures. The role of diameter and interparticle spacing has also been defined. The obtained upconversion enhancement was 7 times but differed 3 times than the FEM prediction.

2. An optimized film of commercial Er^{3+} doped $NaYF_4$ has been developed. EBL defined Au nano-discs were placed successfully. Preliminary optical measurements have been done. Additionally, an linking has been established between Au nanorods and UCNP for an Au embedded upconverting thin film.

5.2 Outlook

5.2.1 Chemical synthesis of upconverting nanocrystals

One of the key objectives of this work is to optimize the nanostructures host for the Er^{3+} ions. However my involvement with commercial UCNP as shown in chapter 4 does not allow me to identify the effect of geometry of nanostructures, dopant concentration, type of dopants, etc on UCL. However my active involvement in the synthesis of these UCNP could answer all the above questions. That would result in a true nanostructures optimization as a host for 1500 nm wavelength UCL . Due to the limited involvement in the chemistry at our group here, I have decided to have a 3 months research stay in this winter at the group of Prof. Frank C.J.M. van Veggel, at the University of Victoria, Canada. The plan is to learn the chemical synthesis of different UCNPs (eg. Er^{3+} doped $NaYF_4$, Er^{3+} doped $NaGdF_4$ etc). The luminescence properties of the structures will also be tailored by synthesizing some onion line multilayer UCNPs with several combinations of optically active (Er^{3+}, Tm^{3+} etc) and inactive lanthanide ions (Gd^{3+} and Y^{3+}), works as a spacer between active ions. The group of Prof. Veggel is actively involve in such inorganic synthesis and this will allow me to receive significant outputs in this short period of time. After learning the synthesis methodology, I will develop a similar synthesis setup in our group at Aarhus University for the preparation of UCNP for my ongoing works defined in chapter 4 of this report. Further, my visit will open up a future collaboration with the groups.

5.2.2 Implementation of an efficient upconverting thin film into commercially available solar cells and further photo-current measurements

This work will be performed in the last year of my PhD where I will assemble the plasmonically enhanced upconverting layer on the back of the bi-facial silicon and organic solar cells. Under SUNTUNE project, the collaboration has been established with a German and a Danish solar cells production companies to receive bi-facial silicon solar cells for this purpose. Regarding the organic solar cells, we have a collaboration with the group of Dr. Morten Madsen which is actively involve on this research. We will need a new numerical model where complete cell is in consideration and that will give the new parameters for Au nanostructures and the exact position of the upconverting film in both kind of solar cells. Currently Emil, a PhD in our group is working on this. After optimizing this new plasmonically enhanced upconverting film,I will be involved in its adhesion to the available solar cells and its photo-current measurements to see the actual impact of this enhanced upconversion on the industrial solar cells.

Bibliography

[1] Solar Generation: Solar Photovoltaic Electricity Empowering the World, European Photovoltaic Industry Association—EPIA, 2011.

[2] World Energy Assessment Report: Energy and the Challenge of Sustainability, United Nations Development Program, United Nations, New York (USA), 2000, 162.

[3] H. A. Atwater and A. Polman, Plasmonics for improved photovoltaic devices, Nat. Mater., 2010, 9, 205.

[4] A. J. Nozik and J. Miller, Introduction to solar photon conversion, Chem. Rev., 2010, 110, 6443.

[5] P. K. Nayak, G. Garcia-Belmonte, A. Kahn, J. Bisquert and D. Cahen, Photovoltaic efficiency limits and material disorder, Energy Environ. Sci., 2012, 5, 6022.

[6] X. Huang, S. Han, W. Huang and X. Liu, Enhancing solar cell efficiency: the search for luminescent materials as spectral converters, Chem. Soc. Rev. 2013, 43, 173.

[7] S. Fischer, J. C. Goldschmidt, P. Loper, G. H. Bauer, R. Brüggeman, K. Kramer, D. Biner, M. Hermle and S. W. Glunz, Enhancement of silicon solar cell efficiency by upconversion: Optical and electrical characterization, J. Appl. Phys. 2010, 108, 044912.

[8] F.Auzel, Upconversion and Anti-Stokes Processes with f and d ions in Solids, Chem.Rev., 2004, 104, 139.

[9] S. R. Johannsen, S. P. Madsen, B.R. Jeppesen, J. V. Nygaard, B. Julsgaard, P. Balling, and A. Nylandsted Larsen, Up-conversion enhancement in Er^{3+} doped TiO_2 through plasmonic coupling: Experiments and finite-element modeling, Appl. Phys. Lett. 2015, 106, 053101.

[10] A. E. Christensen, C. Uhrenfeldt, B. Julsgaard, P. Balling, and A. Nylandsted Larsen, Interaction between Au nanoparticles and Er^{3+} ions in a TiO_2 matrix: Up-conversion of infrared light, J. Egypro. 2011, 10, 111.

[11] H. Mertens, and A. Polman, Plasmon-enhanced erbium luminescence, Appl. Phys. Lett. 2006, 89, 211107.

[12] H.P. Paudel, D. Dachhepati, K. Bayat, S.S. Mot- taghian,P.S. May, C. Lin, S. Smith, and M.F. Baroughi, Design, fabrication, and characterization of a plasmonic upconversion enhancer and its prospects for photovoltaics, J. Photon. Energy., 2013, 23, 035598.

[13] J. C. Goldschmidt, S. Fischer, H. Steinkemper, F. Hallermann, G. von Plessen, K. W. Kramer, D. Biner, and M. Hermle, Increasing Upconversion by Plasmon Resonance in Metal Nanoparticles—A Combined Simulation Analysis, IEEE J. OF Photovol., 2012, 2(2), 134.

[14] S. Fischer, F. Hallermann, T. Eichelkraut, G. von Plessen, K. W. Krämer, D. Biner, H. Steinkemper, M. Hermle, and J. C. Goldschmidt, Plasmon enhanced upconversion luminescence near gold nanoparticles – simulation and analysis of the interactions: Errata, Opt. Exp. 2013, 21(9), 10606.

[15] A. Agrawal, I. Kriegel, and D. J. Milliron, Shape-Dependent Field Enhancement and Plasmon Resonance of Oxide Nanocrystals, J. Phys. Chem. C, 2015, 119 (11), 6227.

[16] I. Zoric, M. Zach, B. Kasemo, and C. Langhammer,Gold, Platinum, and Aluminum Nanodisk Plasmons: Material Independence, Subradiance, and Damping Mechanisms, ACS Nano, 2011, 5, 2535.

[17] C. Noguez, Surface Plasmons on Metal Nanoparticles: The Influence of Shape and Physical Environment, J. Phys. Chem. C., 2007, 111, 3806.

[18] A. Patra, C.S. Friend, R. Kapoor and P.N. Prasad, Fluorescence upconversion properties of Er^{3+} -Doped TiO_2 and $BaTiO_3$ nanocrystallites, Chem. Mater. 2003, 15, 3650.

[19] S.-Y. Chen, C.-C. Ting and W. -F. Hsieh, Copmarison of visible fluorescence properties between sol-gel derived Er^{3+}-Yb^{3+} and Er^{3+}- Yb^{3+} co-doped TiO_2 films, Thin Solid Film, 2003, 434, 171.

[20] C. Li , Z. Quan , J. Yang , P. Yang , and J. Lin, Highly Uniform and Monodisperse β - $NaYF_4$:Ln^{3+} (Ln = Eu, Tb, Yb/Er, and Yb/Tm) Hexagonal Microprism Crystals-: Hydrothermal Synthesis and Luminescent Properties, Inorg. Chem., 2007, 46 (16), 6329.

[21] S. Heer, K. Kömpe, H.-Ulrich Güdel,and M. Haase, Highly Efficient Multicolour Upconversion Emission in Transparent Colloids of Lanthanide-Doped NaYF$_4$ Nanocrystals., Adv. Mater., 2004, 16, 2102.

[22] D. Chen, P. Huang, Y. Yu, F. Huang, A. Yang and Y. Wang, Dopant-induced phase transition: a new strategy of synthesizing hexagonal upconversion NaYF$_4$ at low temperature, Chem. Commun., 2011, 47, 5801.

[23] M.Haase and H. Schäfer, Upconverting Nanoparticles, Angew Chem Int Ed, 2011, 50, 5808.

[24] F. Zhang, R. Che, X. Li, C. Yao, J. Yang, D. Shen, P. Hu, W. Li, and D. Zhao, Direct Imaging the Upconversion Nanocrystal Core/Shell Structure at the Subnanometer Level: Shell Thickness Dependence in Upconverting Optical Properties, Nano Lett., 2012, 12 (6), 2852.

[25] S.A.Maier, Plasmonics:Fundamentals and Applications, 2007, USA:Springer.

[26] W.A.Murray and W.L.Barnes, Plasmonic Materials, adv.Mat., 2007, 19(22),3771.

[27] M.Ohring, Materials Science of Thin Films: Depostion and Structure, London, England:Elsevier 2002.

[28] S. P. Madsen, S. R. Johannsen, B. R. Jeppesen, J. V. Nygaard, P. B. Jensen, J. Chevallier, B. Julsgaard, P. Balling, A. Nylandsted Larsen, Optimizing Plasmonically Enhanced Upconversion, Energy Procedia 2015, 77, 478.

[29] P.B. Johnson, and R.W. Christy, Optical Constants of the Noble Metals,Phys.Rev.B., 1972, 6, 4370.

[30] I.H.Malitson, Interspecimen Comparison of the Refractive Index of Fused Silica, J.Opt.Soc.Am. 1965, 55, 1205.

[31] S. Fischer, H. Steinkemper, P. Löper, M. Hermle1 and J.C. Goldschmidt, Modeling upconversion of erbium doped microcrystals based on experimentally determined Einstein coefficients, J. Appl. Phys. 2012, 111, 013109.

[32] F Chen, W Bu, Y Chen, Y Fan, Q He, M Zhu, Superparamagnetic Fe_3O_4@SiO_2 T_2-weighted MRI contrast agent: highly reproducible synthesis of uniform single-loaded core-shell nanostructures, Chem Asian J, 2009, 4,1809-16.

[33] M. Saboktakin, X. Ye, S. Ju Oh, S.-H. Hong, A. T. Fafarman, U. K. Chettiar, N. Engheta, C. B. Murray, and C. R. Kagan, Metal-Enhanced Upconversion Luminescence Tunable through Metal Nanoparticle–Nanophosphor Separation, ACS Nano, 2012, 6 (10), 8758.

[34] S. K Ram, R. Rizzoli, D. Desta, B. R Jeppesen, M. Bellettato, I. Samatov, Y.-C. Tsao, S. R Johannsen, P. T Neuvonen1, T. G. Pedersen, Directly patterned TiO_2 nanostructures for efficient light harvesting in thin film solar cells, J. Phys. D: Appl. Phys., 2015, 48, 365101.